Contents lists available at GrowingScience

Current Chemistry Letters

homepage: www.GrowingScience.com

The quantum chemical study of the reaction between chlorocarbonylsulfenyl chloride and benzamide

Zakaria Jalil[a], El hassan El -Karni[a], M'hamed Touil[b], Mohamed M'barki[a] and Mustapha Oubenali[a*]

[a]*Team of Analytical & Computational Chemistry, Nanotechnology and Environment, Faculty of Science and Technologies, Sultan Moulay Slimane University, BP 523, Beni Mellal, Morocco*
[b]*Materials Science and Sustainable Energy Laboratory, Department of Chemistry, Faculty of Science, Abdelmalek Essaadi University, B.P. 2121, M'Hannech II, 93030 Tétouan, Morocco*

C H R O N I C L E

Article history:
Received July 18, 2024
Received in revised form
August 15, 2024
Accepted October 7, 2024
Available online
October 7, 2024

Keywords:
DFT
NBO analysis
TST
ClCOSCl
$PhCONH_2$

A B S T R A C T

Using a regioselectivity descriptor known as Fukui indices, this theoretical study examines the reactivity of cycloaddition processes of benzamide ($PhCONH_2$) and chlorocarbonylsulfenyl chloride (ClCOSCl) at the level of base 6-311 G (d. p) by use of the DFT approach. Therefore, the attack of the sulfur atom on nitrogen and carbon on oxygen is kinetically more preferred than the assault of the sulfur atom on oxygen and carbon on nitrogen, as we have observed from our study. The electrophilic Δω difference between chlorocarbonylsulfenyl chloride and benzamide is 1.3726 eV. This indicates that the reaction under investigation has a polar nature (Δω > 1). on oxygen and carbon on nitrogen, as we have observed from our study. We have also studied the stereoselectivity and feasibility of these reactions from a thermodynamic and orbital point of view. The transition states of this reaction have been determined.

1. Introduction

Aromatic heterocycles are the cornerstone of contemporary organic synthesis and are highly valued instruments in the production of agrochemicals, organic materials, and medications in both scholarly and commercial contexts [1-6].

Isothiazoles are an important class of sulfur-containing five-membered aromatic heterocyclic, widely used in crop protection products and chemical synthesis [7]. The isothiazole ring can also be used to construct a wide variety of bioactive chemicals; for example, compounds with anti-poliovirus action have been created [8]. In addition, promising compounds for the treatment of Parkinson's disease have been discovered [9], as well as derivatives that could treat diabetes [10] and cancer [11].

In addition, a thorough review of the literature on metal-organic hybrid complexes is presented, including practical applications and results of these hybrid complexes as catalysts for cross-linking reactions in aqueous and hydroalcoholic environments (also known as "green chemistry") [12].

The aim of the current work is to determine the reactivity of the cycloaddition reaction between benzamide and chlorocarbonylsulfenyl chloride to produce 1, 3, 4-oxathiazole-2-ones, an isothiazole derivative. The research uses a sophisticated computational technique, in particular density functional theory (DFT), which is the most relevant approach in quantum chemistry and allows a precise theoretical study of the electronic structure at the 6-311G (d, p) basis level.

As a first step, we therefore carried out a number of calculations to examining the reactivity of benzamide and chlorocarbonylsulfenyl chloride using quantum mechanical calculations at the DFT level (B3LYP), utilizing global and

* Corresponding author
E-mail address mustapha.oubenali@gmail.com (M. Oubenali)

doi: 10.5267/j.ccl.2024.10.005

local chemical reactivity descriptors. These descriptors shed light on the charge transfer between the molecules of benzamide and chlorocarbonylsulfenyl chloride and offer crucial information on the electrical structure. Subsequently, more sophisticated calculations were carried out to rationalize the reaction studied in this study (**Fig. 1**) from the point of view of transition state theory (TST) and thermodynamics, including the determination of the variations in reaction energy ΔEr, reaction enthalpy (ΔHr), reaction free enthalpy (ΔGr), ZPE ("zero-point energy") and entropy variation (ΔSr).

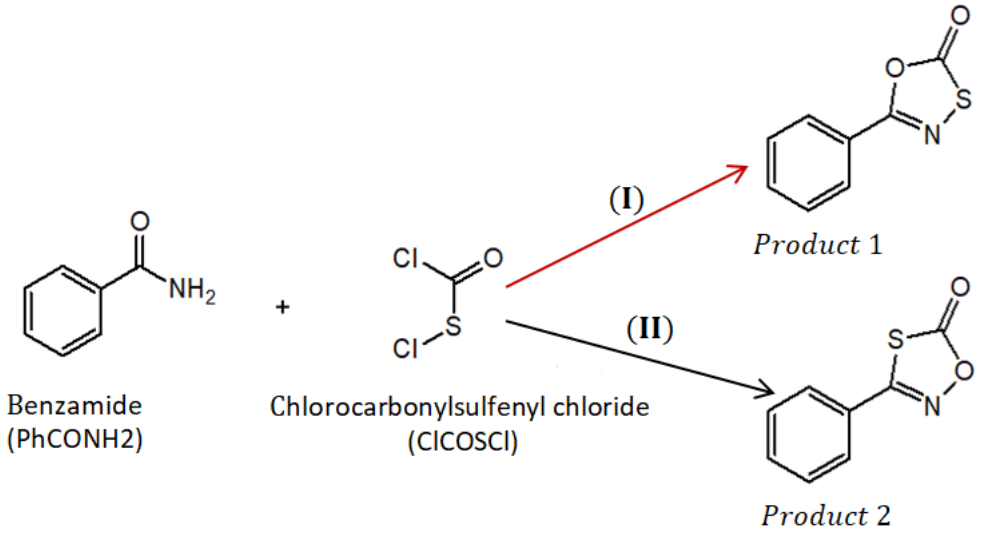

Fig. 1. Geometric structures of the studied molecules

2. Calculation methods

In the field of quantum chemistry, chemical phenomena are explained using deductive reasoning using the principles of quantum mechanics. DFT is one of the most often utilized techniques in quantum computing. Important details about the stability of molecular structure and reactivity are provided by this approach [13–17].

An essential notion in the Conceptual Density Functional Theory (DFT) framework is electronegativity, which is the first derivative of energy (E) relative to the total amount of electrons N. The following connection [18] illustrates how Parr and Pearson demonstrated that the second derivative of energy is equivalent to the negative of the chemical potential μ.

$$\chi = -\left(\frac{\partial E}{\partial N}\right) \qquad \chi = -\left(\frac{I+A}{2}\right)$$

$$\mu = -\chi = \left(\frac{\partial E}{\partial N}\right)_{v(r)}$$

$$\mu = \frac{(\varepsilon_{HOMO} + \varepsilon_{LUMO})}{2}$$

The second derivative of energy E with respect to N is called apparent hardness, another important parameter for understanding structure and reactivity, is given by the following formula[19]:

$$\eta = \left(\frac{\partial^2 E}{\partial N^2}\right)_{v(r)} = \left(\frac{\partial \mu}{\partial N}\right)_{v(r)}$$

$$\eta = (\varepsilon_{LUMO} - \varepsilon_{HOMO})$$

Parr and al defines the electrophilic index as [20-24]: $\omega = \frac{\mu^2}{2\eta}$

When the system exchanges an electronic charge, ΔN, with the environment, this index measures the energy stabilization that occurs. This characteristic describes a molecule's electrophilic power and electron-absorbing tendency. There have been numerous significant attempts to define an inherent nucleophilic index as a theoretical quantity. The empirical nucleophilic index is defined by the following equation in accordance with the Kohn-Sham scheme [22-26]:

$$\mathrm{N} = \mathrm{E}_{\mathrm{HOMO(Nu)}} - \mathrm{E}_{\mathrm{HOMO(TCE)}}$$

Tetracyanoethylene (TCE) is taken as a reference because of its lower HOMO energy in a large series of molecules. In this scale, the nucleophilicity index of TCE is E_{HOMO} (TCE) = -0.335198. Hartree calculated with DFT-B3LYP/6-311G (d, p). Another way of obtaining information on the charge transfer process and measurements on the binding property of atoms is through the fraction of electron transferred (ΔN), this parameter can be obtained by applying the formula[20,27]:

$$\Delta N_{max} = -\frac{\mu}{\eta}$$

To predict the local (site) reactivity (selectivity) of a chemical species, other local reactivity descriptors have also been proposed, such as Parr functions (P_k), local nucleophilicity condensed at atom k (N_k) and local electrophilicity index condensed at atom k (ω_k). These parameters are given respectively by the equations [28,29]:

$$N_k^- = N.P_k^-$$

$$\omega_k^+ = \omega.P_k^+$$

3. Results and discussions

3.1. Geometry and optimized structures of the studied molecules

To determine the most stable conformation of each component, we first optimized the molecular structures of the chemicals used as reactants in the reaction described in **Fig. 1**. We used the B3LYP/6-311G (d, p) gas-phase model to further optimize the optimal conformation, then, using the self-consistent reaction field approach and the polarizable continuum model (PCM) with a dielectric constant of 78.39, solvent effects were taken into consideration (**Fig. 2**). These molecules all have geometries optimized for the singlet spin state, with no symmetry restrictions. A Hessian calculation was performed with Gaussian software to determine all stationary points as minima (no imaginary frequencies).

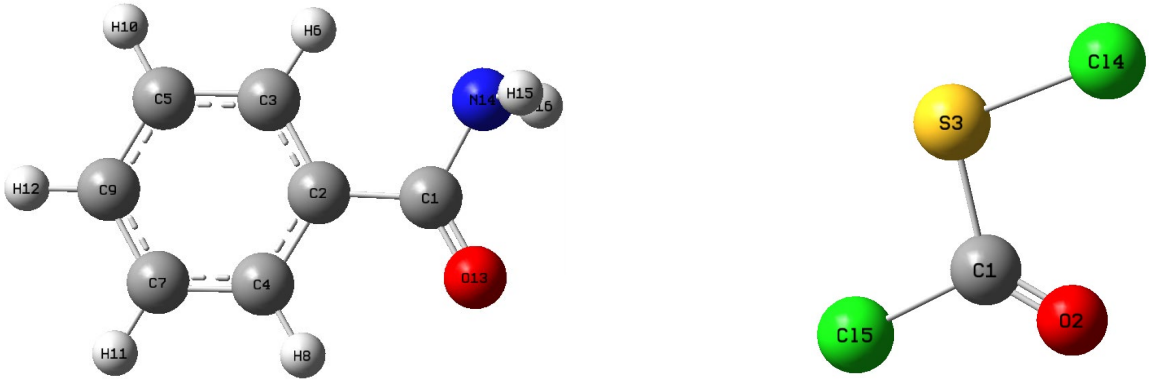

$PhCONH_2$ ClCOSCl

Fig. 2. Optimized structures of the reactive molecules studied

3.2. Prediction of electrophilic/nucleophilic character of reagents

All of the electronic characteristics of the reactive molecules were computed at B3LYP/6-311G (d, p) levels while accounting for the solvent's influence using the self-consistent reaction field technique and the polarisable continuous model (PCM), which has a dielectric constant of 78.39. **Table 1** provides a summary of the outcomes.

Table 1. Electronic properties of the molecules studied calculated at the level B3LYP/6-311G (d, p)

Molecule	HOMO (eV)	LUMO (eV)	μ (eV)	η (eV)	ω (eV)	N (eV)	ΔN_{max}
ClCOSCl	-7.96	-3.05	-5.55	9.18	1.68	1.15	1.12
$PhCONH_2$	-7.30	-1.52	-4.37	9.70	0.98	1.81	0.76

In the case of the reaction between $PhCONH_2$ and ClCOSCl , the chemical electron potential of $PhCONH_2$ (μ = -4.37 eV) is higher than that of ClCOSCl (μ = -5.55 eV), indicating that electron transfer will take place from $PhCONH_2$ to ClCOSCl, this result is well confirmed by the high value of the nucleophilicity of molecule $PhCONH_2$ (N = 1.81 eV) . On the other hand, the overall electrophilic index of $PhCONH_2$ (ω = 0.98 eV) is lower than that of the reagent ClCOSCl (ω = 1.68 eV), meaning that the reagent ClCOSCl behaves as an electrophile, while $PhCONH_2$ behaves as a nucleophile.

To demonstrate the polar nature of the reactions and the donor (nucleophilic) or acceptor (electrophilic) characteristics of the reagents. We computed the reagents' HOMO/LUMO energy differences and electrophilicity variations (**Table 2**).

Table 2. Electrophilique Difference of the reactants Δω

Reagents	$\left\|E_{LUMO}^{PhCONH2} - E_{HOMO}^{ClCOSCl}\right\|$	$\left\|E_{LUMO}^{ClCOSCl} - E_{HOMO}^{PhCONH2}\right\|$	Δω (eV)
$PhCONH_2$ + ClCOSCL	10.4	8.5	1.9

The difference between the electrophilic indices of the two reagents being greater than 1 (Δω>1) means that the reaction studied is polar in nature, as indicated by their predicted value of 1.9 eV (Table 2) [30].

3.3. Molecular electrostatic potential

Electrostatic interactions in a variety of chemical systems are typically represented by the molecular electrostatic potential (MEP). Using the optimized DFT-B3LYP/6-311G (d, p) geometry, the MEP for ClCOSCl and $PhCONH_2$ was calculated. The surface map produced is shown in **Fig. 3**. A color code is used in this graph to indicate electrostatic potential values. Red highlights the highest negative potential and indicates areas likely to be subject to electrophilic attack. On the other hand, regions with the highest positive charge are shown in dark blue, indicating where nucleophiles prefer to attack. As can be seen in, the intermediate color gradient changes from red to orange, yellow, green and blue. The limits set for the $PhCONH_2$ and ClCOSCl molecules are -4.676e-2 and -3.632e-2 (deepest red) and 4.676e-2 and 3.632e-2 (deepest blue).

In the case of the $PhCONH_2$ molecule, the most negative electrostatic potential is mainly found around the oxygen atom, while positive potentials are located near the nitrogen atom. For the ClCOSCl molecule, the positive and negative potentials are located on the oxygen and carbon atoms respectively. In summary, the MEP indicates a probable electrophilic attack on the oxygen atom of $PhCONH_2$ by the carbon atom of the ClCOSCl molecule. Conversely, a strong nucleophilic attack is anticipated on the nitrogen atom of $PhCONH_2$ by the sulfur atom of ClCOSCl.

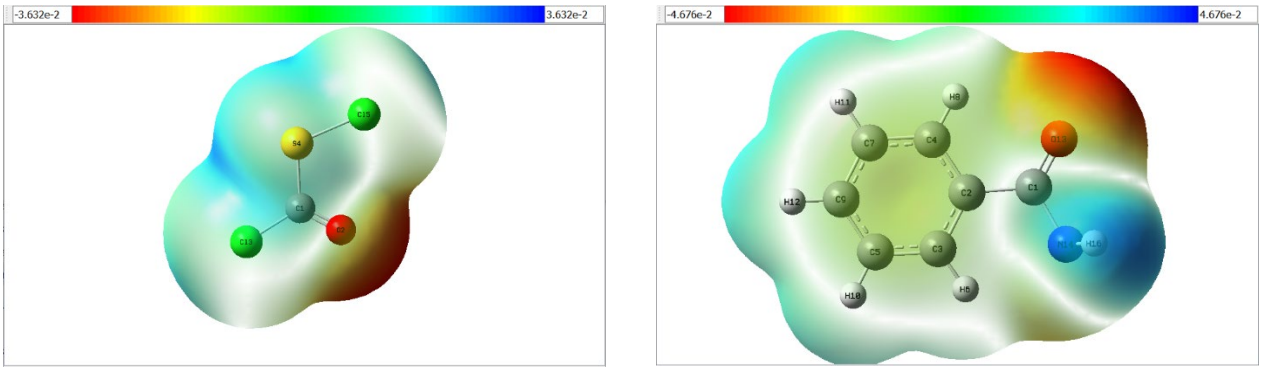

Fig. 3. Mapping the electrostatic potential around the four molecules

3.4. Prediction of the local reactivity of reagents

The Fukui and Parr functions of the $PhCONH_2$ and ClCOSCl molecules were evaluated to better understand their reactivity and their electron donor and acceptor characteristics. These functions, f^+ and p_k^+, show the electrophilic behaviors and f^- and p_k^- the nucleophilic behaviors of the molecules. **Fig. 4** shows a graphical analysis of the Fukui indices, while Table 3 summarizes the values of the Parr functions**. Fig. 4** show the electrophilic nature of ClCOSCl and the nucleophilic character of the $PhCONH_2$ molecule. At the same time, the indices of local electrophilicity and local nucleophilicity are considered to be among the best parameters for qualifying and predicting the reactivity and regioselectivity of a molecule in terms of chemical bonding. It occurs between the most electrophilic sites (indicated by the highest w^+ value) and the most nucleophilic sites (indicated by the highest N^- value) of the molecules that come into contact with each other.

A detailed examination of **Fig. 4** reveals that the O13, C1 and C9 atoms of the $PhCONH_2$ molecule will be the preferred sites for electrophilic attack, while the N14 nitrogen atom will be the favored site for nucleophilic attack. Similarly, the nucleophilic and electrophilic centers of the ClCOSCl molecule are mainly located in the sulfur (S4) and chlorine (Cl4) atoms. These two atoms each play a dual role in reactions based on electron transfer. The results presented in **Table 2** confirm these conclusions. Indeed, According to **Table 2**, significant values of 0.20, 0.21, and 0.19, respectively, are found for the $\boldsymbol{p_k^-}$ function on the O13, C1, and C9 atoms. Furthermore, the nitrogen atom (N14) has a significant value of 0.21 for the $\boldsymbol{p_k^+}$ function. This analysis clearly shows that the electrophilic centre of the $PhCONH_2$ molecule is centred around the nitrogen atom, while the nucleophilic centres are the O13, C1, and C9 atoms. The $\pi_{C=N}$ bond is highly polar, and polar bonds are excellent electron pair acceptors (electrophiles), due to electron delocalization in the conjugated molecules. This mesomeric effect gives the nitrogen atom a partial positive charge. The most favorable interaction between $PhCONH_2$ and

ClCOSCl occurs between the (O13) and (N14) atoms of $PhCONH_2$ (possessing a high N^- value) and the (Cl3) and (S4) atoms of ClCOSCl (high w^+ value).

Table 3. Local electrophilic and nucleophilic power of the atoms of $PhCONH_2$ and ClCOSCl obtained by a calculation of the Fukui indices

molecule	atom	Hirshfeld index			
		p_k^+	p_k^-	w^+	N^-
$PhCONH_2$	1 C	0.00	**0.21**	0.00	**0.38**
	2 C	0.04	0.10	0.04	0.19
	3 C	0.05	0.09	0.04	0.17
	4 C	0.17	0.12	0.17	0.22
	5 C	0.17	0.01	0.17	0.03
	7 C	0.04	0.00	0.04	0.00
	9 C	0.02	**0.19**	0.02	**0.34**
	13 O	0.26	**0.20**	0.26	**0.36**
	14 N	**0.21**	0.04	**0.21**	0.08
ClCOSCl	1 C	-0.02	0.11	-0.04	0.13
	2 O	0.23	0.04	0.38	0.05
	3 Cl	0.00	0.10	0.00	0.12
	4 S	0.53	0.37	0.90	0.43
	5 Cl	0.25	0.35	0.43	0.41

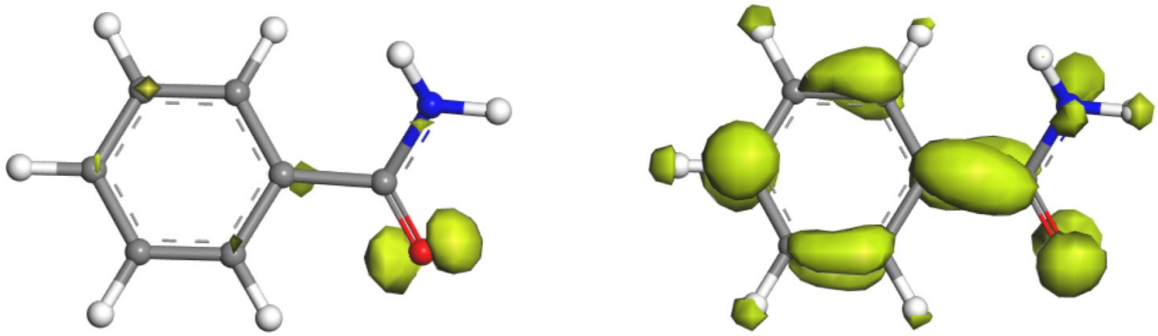

Fig. 4. $PhCONH_2$ compound's simulated Fukui indices, f^- (left) and f^+ (right)

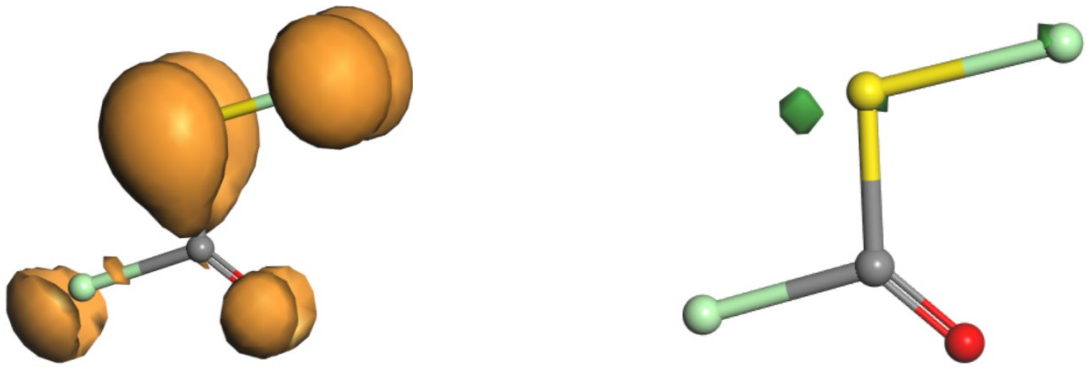

Fig. 5. ClCOSCl compound's simulated Fukui indices, f^- (left) and f^+ (right)

3.5. Thermodynamic analysis

We have examined the possibility of reactions between $PhCONH_2$ and ClCOSCl, involving electron transfer between the reactive molecules, from the point of view of frontier orbital theory. We plan to use the thermodynamic technique in this section to gather more information on this reaction and provide an explanation for the resulting majority and minority products. In this regard, we have computed the changes in reaction energy ΔE_r, enthalpy of reaction ΔH_r, free enthalpy of reaction ΔG_r, ZPE ("zero-point energy"), thermal energy ΔQ_r variation and entropy change ΔS_r that correspond to reactions I and II under standard temperature and pressure circumstances (T = 298.15 K; P = 1 atm).

Reactions I and II appear spontaneously thermodynamically favorable, and both reactions are exothermic, as shown in **Table 4**. All changes in the free enthalpy of reaction ΔG_r and the change in thermal energy are negative. Furthermore, since the predicted thermochemical properties of reaction I are more valuable than those of reaction II, we find that reaction I is the thermodynamically preferred reaction. In reaction II, the entropy change is negative, suggesting an increase in order,

while for reaction II, the value is positive, indicating a decrease in order. This conclusion indicates that there are more moles of product 1 than product 2, which explains the increase in entropy of the system in reaction I, indicating that reaction I is preferred to reaction II.

Table 4. Calculated values ($Kcal.mol^{-1}$) of reaction energy changes and ZPE ($\Delta E_r + ZPE$), reaction free enthalpy changes ΔG_r, reaction enthalpy changes ΔH_r, thermal energy ΔQ_r variation and the entropy variation ΔS_r ($cal.\,mol^{-1}K^{-1}$)

Reactions	$\Delta E_r + ZPE$	ΔH_r	ΔG_r	ΔQ_r	ΔS_r
Reaction (I)	-5.9	-5.8	-6.9	-4.1	3.6
Reaction (II)	-2.5	-2.6	-1.9	-4.0	-2.1

3.6. Analysis of the potential energy surface

The geometries of both the ground state and transition state have been completely optimized using the DFT (B3LYP) method with the 6-311G (d, p) basis set, which is accessible within the Gaussian software. Frequency calculations were conducted for these geometries, with the transition state exhibiting an imaginary frequency that corresponds to the reaction coordinate. The structure and normal mode vibrations have been visualized using GaussView 6.

To highlight the type of nucleophilic attack on the sulfur and carbon atoms of ClCOSCl on the nitrogen and oxygen atoms of $PhCONH_2$, we determined the energies of the reactants, the products, and the transition states, as well as the energy of the reaction between $PhCONH_2$ and ClCOSCl. **Fig. 6** shows the energy profile of the reaction between $PhCONH_2$ and ClCOSCl. The potential energy surface indicates that the energy of the transition state corresponding to the attack of the sulfur and carbon atoms on the nitrogen and oxygen, respectively, is lower than the energy of the transition state corresponding to the attack of sulfur and carbon on oxygen and nitrogen, respectively (**Fig. 6**). The activation energies corresponding to the two modes of attack are E_a=9.3 kcal/mol for TS1 and E_a=25.5 kcal/mol for TS2 . Thus, the attack of the sulfur atom on nitrogen and carbon on oxygen is kinetically more favorable than the attack of sulfur on oxygen and carbon on nitrogen (**Table 5**).

The thermochemical functions of the reactions (ΔH, ΔS and ΔG) were obtained from thermochemical calculations and are reported in Table 5. As can be seen, the Gibbs free energy barrier for the formation of TS in reaction 1 is 60.2 kcal mol^{-1}, while the calculated value in reaction 2 is 61.6 kcal mol^{-1} which reflects the stability of product 1 compared to product 2.

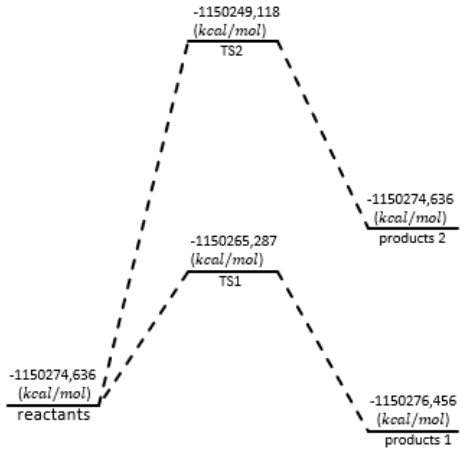

Fig. 6. Energy profile for the reaction studied

Table 5. Calculated kinetic and activation parameters at 298.15K corresponding to the formation of the two products calculated by the DFT method B3LYP/6-311G (d. p)

	ΔH (kcal/mol)	**ΔG (kcal/mol)**	**ΔS (cal/mol.k)**	**ΔE (kcal/mol)**	**E_a (kcal/mol)**
Reaction I	96.8	60.2	124.9	96.8	9.3
Reaction II	97.6	61.6	120.7	97.0	25.5

The two transition state structures optimized by DFT B3LYP/6-311G (d. p) that are involved in the two reactions are shown in **Fig. 7.**

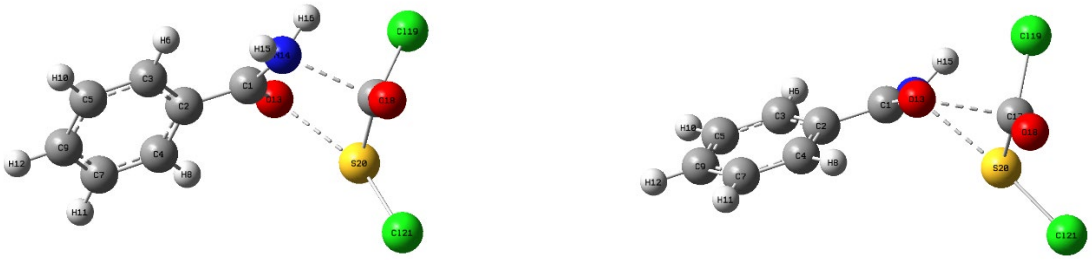

TS1 TS2

Fig.7. Structures of the transition states obtained by DFT B3LYP/6-311G (d. p) involved in the reactions studied

3.7. NBO Analysis

The analysis of natural bonding orbitals (NBO) provides an effective method for studying intramolecular interactions, rehybridization, and the delocalization of electronic density within a molecule. It is also used to evaluate different types of donor-acceptor interactions and their stabilization energies.

In the context of NBO analysis, the focus is on donor-acceptor interactions, specifically bond-antibond relationships, by evaluating all potential interactions between "occupied" Lewis-type NBOs (acting as donors) and "unoccupied" non-Lewis NBOs (serving as acceptors). The energies associated with these interactions are subsequently calculated using second-order perturbation theory. These interactions, which contribute to stabilization, are termed "delocalization" corrections to the natural Lewis structure.

Table 6. Second order perturbation theory analysis of the Fock matrix in NBO basis in products 1 and 2.

Molecule	Donor	Type	ED/e	Acceptor	Type	ED/e	E(2)	E(j)-E(i)	E(i, j)
Product 1	C2-C3	π	1.63800	C1-N14	π*	0.25498	26.91	0.23	0.072
	C2-C3	π	1.63800	C4-C7	π*	0.28972	20.16	0.28	0.069
	C2-C3	π	1.63800	C5-C9	π*	0.31710	18.40	0.28	0.065
	C4-C7	π	1.65915	C2-C3	π*	0.38457	19.73	0.27	0.066
	C4-C7	π	1.65915	C5-C9	π*	0.31710	21.36	0.28	0.069
	C5-C9	π	1.98049	C2-C3	π*	0.38457	18.72	0.28	0.066
	O13	Lp(2)	1.76056	C1-N14	π*	0.25498	32.73	0.33	0.093
	O13	Lp(2)	1.76056	C15-O16	σ*	0.30085	36.67	0.31	0.096
	N14	Lp(1)	1.93402	C1-O13	σ*	0.07335	12.10	0.69	0.089
	O16	Lp(2)	1.77352	O13-C15	σ*	0.13751	35.17	0.5	0.123
	O16	Lp(2)	1.77352	C15-S17	σ*	0.16520	39.08	0.33	0.103
	S17	Lp(2)	1.78175	C15-O16	σ*	0.30085	26.82	0.22	0.070
	C1-N14	π	1.95746	C2-C3	π*	0.38457	42.63	0.05	0.072
	O13-C15	σ	1.98560	C1-O13	σ*	0.07335	44.44	0.01	0.061
Product 2	C1-N14	π	1.82198	C15-O16	π*	0.30819	34.67	0.32	0.097
	C2-C3	π	1.62055	C1-N14	π*	0.33876	31.06	0.23	0.076
	C2-C3	π	1.62055	C4-C7	π*	0.01539	20.39	0.28	0.070
	C2-C3	π	1.62055	C5-C9	π*	0.01705	17.88	0.28	0.064
	C4-C7	π	1.64784	C2-C3	π*	0.38966	19.30	0.27	0.065
	C4-C7	π	1.64784	C5-C9	π*	0.01705	22.13	0.28	0.070
	C5-C9	π	1.63036	C2-C3	π*	0.38966	24.09	0.27	0.073
	C5-C9	π	1.63036	C4-C7	π*	0.01539	17.93	0.28	0.065
	O13	π	1.99979	C1-N14	π*	0.33876	44.52	0.31	0.109
	N14	Lp(1)	1.82946	C1-O13	σ*	0.07281	15.79	0.62	0.091
	N14	Lp(1)	1.82946	C15-S17	σ*	0.31408	20.45	0.35	0.079
	O16	Lp(2)	1.74880	N14-C15	σ*	0.06464	16.15	0.70	0.100
	O16	Lp(2)	1.74880	C15-S17	σ*	0.31408	66.06	0.20	0.121
	S17	Lp(1)	1.99015	C15-O16	σ*	0.30819	14.26	0.23	0.054

The NBO calculations were conducted utilizing the DFT - B3LYP/6-311G (d, p) methodology. The details regarding the occupation and energies of orbitals i and j, as well as the E(2) values for Lp(1), Lp(2), and the transitions from bond to antibond ($\sigma/\pi \rightarrow \sigma^*/\pi^*$), are summarized in **Table 6**. For molecule 1, the interaction Lp(2) (O16) → σ** (O13-C15) resulted in a maximum ΔE_{ij} of 36.26 kcal/mol. In contrast, for molecule 2, the interaction Lp(2) (O16) → σ* (C15-S17) yielded a maximum ΔE_{ij} of 49.18 kcal/mol. Additionally, the transitions from bonding to antibonding states ($\sigma/\pi \rightarrow \sigma^*/\pi^*$) played a crucial role in the structural stability, with maximum contributions of 24.23 kcal/mol and 34.67 kcal/mol for the π (C2-C3) → π* (C1-N14) and π (C1-N14) → π* (C15-O16) interactions in products 1 and 2, respectively. Furthermore, the

polarization of the NBO bond and the corresponding changes in hybridization resulting from the formation of the complexes are examined. The percentage variations observed in the title compound are presented in **Table 6**.

The data presented in **Table 7** indicates that the hybrid orbital O13 in the σ (O13-C15) bond exhibits 35.11% s-character and 64.81% p-character, corresponding to an $sp^{2.57}$ hybridization. The π (C2-C3) bond, characterized by a purely p-character hybrid orbital, functions as the electron donor, while the π* (C1-N14) antibond serves as the electron acceptor [π (C2-C3) → π* (C1-N14)], facilitating a charge transfer quantified at 24.23 kcal/mol for product 1.

In the case of product 2, a significant charge transfer is noted from the π (C1-N14) bond, which also possesses a pure p-character hybrid orbital, to the π* (C15-O16) antibond, with a measured value of 29.11 kcal/mol. Furthermore, the hybrid C1 in the σ (C1-N14) bond demonstrates 35.55% s-character and 64.37% p-character, corresponding to an $sp^{1.81}$ hybrid orbital.

Table 7. Selected NBO results showing formation of Lewis and non-Lewis orbitals for products 1 and 2 by using the DFT method with 6-311G (d, p) basis set.

				%	%s	%p	H.O
Product 1	C2-C3	π	C	53.49	0.00	99.98	p
			C	46.51	0.00	99.95	p
		σ	C	51.56	35.08	64.88	$sp^{1.85}$
			C	48.44	35.34	64.62	$sp^{1.83}$
	C4-C7	π	C	48.74	0.00	99.95	P
			C	51.26	0.00	99.95	P
		σ	C	49.69	36.40	63.56	$sp^{1.75}$
			C	50.31	36.10	63.86	$sp^{1.77}$
	C5-C9	π	C	50.81	0.00	99.96	P
			C	49.19	0.00	99.95	P
		σ	C	49.94	36.05	63.91	$sp^{1.77}$
			C	50.06	36.07	63.89	$sp^{1.77}$
	C1-N14	π	C	37.92	0.00	99.77	P
			N	62.08	0.00	99.81	P
		σ	C	41.05	35.11	64.81	$sp^{1.85}$
			N	58.95	42.70	57.19	$sp^{1.43}$
	O13-C15	σ	O	69.62	28.01	71.92	$sp^{2.57}$
			C	30.38	29.24	70.47	$sp^{2.41}$
Product 2	C1-N14	π	C	34.35	0.00	99.72	P
			N	65.65	0.00	99.83	P
		σ	C	40.92	35.55	64.37	$sp^{1.81}$
			N	59.08	38.76	61.14	$sp^{1.58}$
	C2-C3	π	C	54.32	0.00	99.99	P
			C	45.68	0.00	99.95	P
		σ	C	51.53	35.07	64.89	$sp^{1.85}$
			C	48.47	35.29	64.67	$sp^{1.83}$
	C4-C7	π	C	48.13	0.00	99.95	P
			C	51.87	0.00	99.95	P
		σ	C	61.60	28.64	71.31	$sp^{2.49}$
			C	49.73	36.04	63.91	$sp^{1.77}$
	C5-C9	π	C	51.35	0.00	99.96	P
			C	48.65	0.00	99.95	P
		σ	C	50.06	35.94	64.02	$sp^{1.78}$
			C	49.94	36.03	63.93	$sp^{1.77}$

3.8. Nonlinear optical properties

Properties such as the total dipole moment (μ_{tot}), total polarizability (α_{tot}), and total first hyperpolarizability (β_{tot}) are intrinsically linked to nonlinear optical (NLO) characteristics. The density functional theory (DFT) approach employed in this study has demonstrated its efficacy in analyzing organic materials exhibiting NLO properties. The values we have obtained are compiled in **Table 8**.

The findings suggest that the dipole moment for product 2, measured at 4.9 D, surpasses that of product 1, which implies that product 2 possesses greater stability relative to product 1.

Moreover, the analysis shows that the dipolar polarizability tensor values for both products are equivalent, indicating that they exhibit the same chemical reactivity.

The total first hyperpolarizability (β_{tot}) is determined to be 46.7 D for product 1 and 70.3 D for product 2. This indicates that product 2 experiences enhanced electron delocalization and charge transfer, leading to a more pronounced β response compared to product 1.

Table 8. Electric dipole moment μ, polarizability α and first hyperpolarizability (β) for products 1 and 2 in (Debye)

	Parameters	Product 1	Product 2
Electric dipole moment	μ_x	-3.3	-4.4
	μ_y	-0.7	-1.9
	μ_z	0.0	0.0
	μ_{tot}	**3.4**	**4.9**
polarizability	α_{xx}	-71.3	-71.9
	α_{yy}	-75.4	-74.9
	α_{zz}	-77.1	-77.4
	α_{xz}	-0.0	-0.0
	α_{yz}	-0.0	-0.0
	α_{xy}	-5.7	-7.1
	α_{tot}	**-74.6**	**-74.7**
hyperpolarizability	β_{xxx}	-43.9	-56.4
	β_{xyy}	-18.0	-20.3
	β_{xzz}	16.9	15.0
	β_{yyy}	4.4	-7.5
	β_{xxy}	-20.5	-24.2
	β_{yzz}	3.8	1.3
	β_{zzz}	0.0	0.0
	β_{xxz}	-0.0	-0.0
	β_{yyz}	-0.0	0.0
	β_x	-45.1	-61.9
	β_y	-12.3	-33.4
	β_z	-0.0	-0.0
	β_{tot}	**46.7**	**70.3**

4. Conclusion

In this work, we have demonstrated by DFT method via the standard 6-311G (d, p) basis and the B3LYP functional, the calculation of global indices shows that $PhCONH_2$ acts as nucleophilic donor and ClCOSCl serves as electrophilic acceptor. The difference in electrophilicity is significant, so were talking about a polar process. The reaction to form product 1 is highly exothermic, which shows that this reaction is more favored because the product formed are stable and their formation releases energy, unlike product 2. The results also show that product 1 obtained by addition of the $PhCONH_2$ molecule to the ClCOSCl molecule is more stable and thermodynamically more favorable than product 2. The $PhCONH_2$ molecule has an oxygen atom as its nucleophilic center, while the ClCOSCl molecule has active centers in sulfur and chlorine atoms.

Funding

This research received no external funding.

References

1. Castro. M. Á., Gamito. A. M., Tangarife-Castaño. V., Roa-Linares. V., Miguel del Corral. J. M., Mesa-Arango. A. C., Francesch. A. M., Betancur-Galvis. L., San Feliciano. A. **(2015)**. New 1.4-anthracenedione derivatives with fused heterocyclic rings: synthesis and biological evaluation. *RSC Advances*. 5(2). 1244–1261.
2. Wang. B.-L., Zhu. H.-W., Li. Z.-M., Wang. L.-Z., Zhang. X., Xiong. L.-X., Song. H.-B. **(2017)**. Synthesis. biological evaluation and SAR analysis of novel poly-heterocyclic compounds containing pyridylpyrazole group. *Pest Management Science.* 74(3). 726–736.
3. Jalil Z., El Karni EL H., EL Ouafy T., Echajia M., M'barki M., Oubenali M. **(2023)**. Reactivity of Isothiasole with Dibromine and Sulfuryl Chloride. *Phys. Chem. Res.*11(3). 511-525.
4. Zhang. L., Li. W., Xiao. T., Song. Z., Csuk. R., Li. S. **(2018)**. Design and Discovery of Novel Chiral Antifungal Amides with 2-(2-Oxazolinyl) aniline as a Promising Pharmacophore. *Journal of Agricultural and Food Chemistry.* 66(34). 8957–8965.
5. Wu. Q.-F., Zhao. B., Fan. Z.-J., Zhao. J.-B., Guo. X.-F., Yang. D.-Y., Zhang. N.-L., Yu. B., Kalinina. T., Glukharevab. T. **(2018)**. Design. synthesis and fungicidal activity of isothiazole–thiazole derivatives. *RSC Advances.* 8(69). 39593–39601.
6. Herman. A., Aerts. O., de Montjoye. L., Tromme. I., Goossens. A., Baeck. M. **(2018)**. Isothiazolinone derivatives and allergic contact dermatitis: a review and update. *The European Academy of Dermatology and Venereology*. 33(2). 267–276.

7. Silva. A. D. O., McQuade. J., Szostaka. M. **(2019)**. Recent Advances in the Synthesis and Reactivity of Isothiazoles. *Advanced Synthesis & Catalysis.* 361(13). 3050-3067.
8. Garozzo. A., Stivala. A., Tempera. G., Castro. A. **(2010)**. Antipoliovirus activity and mechanism of action of 3-methylthio-5-phenyl-4-isothiazolecarbonitrile. *Antiviral Research*. 88(3). 325-328.
9. Banerjee, A., Yadav, P. S., Bajpai, M., Sangana, R. R., Gullapalli, S., Gudi, G. S., Gharat, L. A. **(2012)**. Isothiazole and isoxazole fused pyrimidones as PDE7 inhibitors: SAR and pharmacokinetic evaluation. *Bioorg. Med. Chem. Lett*. 22, 3223.
10. Zhang, X., Cai, C., Sui, Z., Macielag, M., Wang, Y., Yan, W., Suckow, A., Hua, H., Bell, A., Haug, P., Clapper, W., Jenkinson, C., Gunnet, J., Leonard, J., Murray, W. V. **(2017)**. Discovery of an Isothiazole-Based Phenylpropanoic Acid GPR120 Agonist as a Development Candidate for Type 2 Diabetes. *ACS Med. Chem. Lett*. 8, 947.
11. Ambati, S. R., Gudala, S., Sharma, A., Penta, S., Reddy, V. L., Bomma, Y., Janapala, V. R., Pola, S. **(2017)**. Facile Synthesis of Novel 3-(4-phenylisothiazol-5-yl)-2H-chromen-2-one Derivatives as Potential Anticancer Agents. *J. Heterocycl. Chem*. 54, 2333.
12. Kletskov. A. V., Bumagin. N. A., Zubkova. F. I., Grudinin. D. G., Potkin. V. I. **(2020)**. Isothiazoles in the Design and Synthesis of Biologically Active Substances and Ligands for Metal Complexes. *Synthesis*. 52(02).159-188.
13. Vektariene. A., Vektaris. G., Svoboda. J. **(2009)**. A theoretical approach to the nucleophilic behavior of benzofused thieno [3.2-b] furans using DFT and HF based reactivity descriptors. *Arkivoc*. (7). 311-329.
14. EL Ouafy. H., Aamor. M., Oubenali. M., Mbarki. M., EL Haimouti. A., EL Ouafy T. **(2022)**. Molecular Structure. Electrostatic Potential and HOMO. LUMO Studies of 4-Aminoaniline. 4-Nitroaniline and 4-Isopropylaniline by DFT. *Science & Technology Asia*. 27(1). 9-19.
15. EL Ouafy. H., EL Ouafy. T., Oubenali. M., EL Haimouti. A., Gamouh. A., Mbarki. M. **(2021)**. Analysis of the Chemical Reactivity of Limonene by the Functional Density Theory Method Using Global Descriptors. *Journal of Chemical Health Risks*. 11(2). 213-221.
16. EL Ouafy, H., Aamor, M., Oubenali, M., Mbarki, M., Gamouh, A., EL Haimouti, A., & EL Ouafy, T. **(2021)**. 4-Bromo-N.N-dimethylaniline. 4-fluoro-N.N-dimethylaniline. 4-methyl-N.N-dimethylaniline: Density-functional theory study. *Science. Engineering and Health Studies.* 15. 21020012.
17. EL Ouafy. H., Aamor. M., Oubenali. M., Mbarki. M., EL Haimouti. A., EL Ouafy. T. **(2022)**. Theoretical study of the stability and reactivity of salicylic acid isomers by the DFT method. *Current Chemistry Letters*. 11(2). 183–190.
18. Parr. R. G., Donnelly. R. A., Levy. M., Palke. W. E. **(1978)**. Electronegativity: The density functional viewpoint. *Chemical Physics*. 68(8). 3801–3807.
19. Parr. R. G., Pearson. R. G. **(1983)**. Absolute hardness: companion parameter to absolute electronegativity. *American Chemical Society*. 105(26). 7512–7516.
20. Parr. R. G., Szentpály. L. v., Liu. S. **(1999)**. Electrophilicity Index. *American Chemical Society*. 121(9). 1922–1924.
21. Chattaraj. P. K., Giri. S. **(2009)**. Electrophilicity index within a conceptual DFT framework. *Royal Society of Chemistry*. 105. 13–39.
22. Domingo. L. R., Ríos-Gutiérrez. M., Pérez. P. **(2016)**. Applications of the Conceptual Density Functional Theory Indices to Organic Chemistry Reactivity. *Molecules.* 21(6). 748.
23. Domingo. L. R., Pérez. P., Sáez. J. A. **(2013)**. Understanding the local reactivity in polar organic reactions through electrophilic and nucleophilic Parr functions. *RSC Adv.* 3(5). 1468.
24. Domingo. L. R. **(2024)**. 1999 – 2024. a Quarter Century of the Parr's Electrophilicity ω Index. *Scientiae Radices*. 3(3). 157-186.
25. Domingo. L. R., Chamorro. E., Pérez. P. **(2008)**. Understanding the Reactivity of Captodative Ethylenes in Polar Cycloaddition Reactions. A Theoretical Study. *Organic Chemistry*. 73(12). 4615–4624.
26. Jaramillo. P., Domingo. L. R., Chamorro. E., Pérez. P. **(2008)**. A further exploration of a nucleophilicity index based on the gas-phase ionization potentials. *Molecular Structure: THEOCHEM*. 865(1-3). 68–72.
27. Domingo. L. R., Pérez. P. **(2013)**. Global and local reactivity indices for electrophilic/nucleophilic free radicals. *Organic and Biomolecular Chemistry*. 11(26). 4350.
28. Domingo. L. R., Pérez. P. **(2013)**. Global and local reactivity indices for electrophilic /nucleophilic free radicals. *Organic & Biomolecular Chemistry,* 11(26), 4350.
29. Ben El Ayouchia, H., Bahsis, L., Anane, H., Domingo, L. R., Stiriba, S. E. **(2018)**. Understanding the mechanism and regioselectivity of the copper(I) catalyzed [3 + 2] cycloaddition reaction between azide and alkyne: a systematic DFT study. *RSC Adv.* 8(14), 7670–7678.
30. Yang. W., Mortier. W. J. **(1986)**. The use of global and local molecular parameters for the analysis of the gas-phase basicity of amines. *J Am Chem Soc*. 108(19). 5708–5711.